

## MIT Open Access Articles

*First Principles Study of the  $\text{Li}_{10}\text{GeP}_2\text{S}_{12}$  Lithium Super Ionic Conductor Material*

The MIT Faculty has made this article openly available. **Please share** how this access benefits you. Your story matters.

**Citation:** Mo, Yifei, Shyue Ping Ong, and Gerbrand Ceder. "First Principles Study of the  $\text{Li}_{10}\text{GeP}_2\text{S}_{12}$  Lithium Super Ionic Conductor Material." *Chemistry of Materials* 24, no. 1 (January 10, 2012): 15-17.

**As Published:** <http://dx.doi.org/10.1021/cm203303y>

**Publisher:** American Chemical Society (ACS)

**Persistent URL:** <http://hdl.handle.net/1721.1/80290>

**Version:** Author's final manuscript: final author's manuscript post peer review, without publisher's formatting or copy editing

**Terms of use:** Creative Commons Attribution-Noncommercial-Share Alike 3.0



# First Principles Study of the $\text{Li}_{10}\text{GeP}_2\text{S}_{12}$ Lithium Super Ionic Conductor Material

Yifei Mo, Shyue Ping Ong, Gerbrand Ceder

Department of Materials Science and Engineering, Massachusetts Institute of Technology, Cambridge, MA 02139

**KEYWORDS:** Lithium ionic conductor, solid electrolyte,  $\text{Li}_{10}\text{GeP}_2\text{S}_{12}$ , *ab initio*, molecular dynamics, phase diagrams

Supporting Information

The continued drive for high performance lithium batteries has imposed stricter requirements on the electrolyte materials.<sup>1,2</sup> Solid electrolytes comprising lithium super ionic conductor materials exhibit good safety and stability, and are promising to replace current organic liquid electrolytes. One major limitation in the application of Li-ion conductors is that their typical conductivity is less than  $10^{-4}$  S/cm at room temperature. Recently, Kamaya *et al.* reported a new Li super ionic conductor  $\text{Li}_{10}\text{GeP}_2\text{S}_{12}$  (LGPS), which has the highest conductivity ever achieved among solid lithium electrolytes of 12 mS/cm at room temperature (comparable conductivity with liquid electrolytes), and outstanding electrochemical performance in Li batteries.<sup>3</sup>

The high conductivity in LGPS is attributed to the fast diffusion of  $\text{Li}^+$  in its crystal structural framework, which consists of  $(\text{Ge}_{0.5}\text{P}_{0.5})\text{S}_4$  tetrahedra,  $\text{PS}_4$  tetrahedra,  $\text{LiS}_6$  octahedra, and  $\text{LiS}_4$  tetrahedra. Kamaya *et al.* proposed that diffusion in LGPS occurs along one-dimension (1D) with diffusion pathways along the *c* axis.<sup>3</sup> The authors also proposed that Li atoms in  $\text{LiS}_4$  tetrahedra enable fast diffusion along the *c* direction, while Li atoms in  $\text{LiS}_6$  octahedra are not active for diffusion. This hypothetical diffusion mechanism in LGPS has been inferred from the large anisotropic thermal factors and the Li disorder in the 1D channels, but has not been directly proven. Understanding this LGPS material is important to improve its performance, and may provide insight into designing new Li super ionic conductor materials.

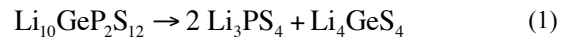
Using first principles modeling, we investigated the diffusivity, stability, and electrochemical window of LGPS. We provide a hypothesis for the observed wide electrochemical window of LGPS. We also identified the diffusion pathways

and calculated the corresponding activation energies and diffusion coefficient.

All calculations in this study were performed using the Vienna *Ab initio* Simulation Package (VASP)<sup>4</sup> within the projector augmented-wave approach.<sup>5</sup> Unless otherwise noted, all calculations were performed using the Perdew-Burke-Ernzerhof generalized-gradient approximation (GGA) to density functional theory (DFT).<sup>6</sup>

We assessed the phase stability of LGPS by constructing the quaternary Li-Ge-P-S phase diagram using all known Li-Ge-P-S compounds in the Inorganic Crystal Structure Database<sup>7</sup>, all  $\text{Li}_x\text{P}_y\text{S}_z$  compounds compiled by Holzwarth *et al.*,<sup>10</sup> and the calculated ground state of LGPS. As the refined structure has partial occupancies, we ordered the arrangement of Li, Ge and P atoms in LGPS using an electrostatic energy criterion.<sup>8</sup> Of the ten orderings with the lowest electrostatic energy, the structure with the lowest calculated DFT energy was selected as the representative ground state. The calculation input parameters are based on those used in the Materials Project<sup>9</sup> to leverage on the large set of computed data available in that database.

Our calculated phase diagram predicts LGPS to be thermodynamically unstable at 0K with respect to the following decomposition:



The calculated  $\text{Li}_3\text{PS}_4$  ground state is iso-structural with  $\beta\text{-Li}_3\text{PO}_4$ , consistent with the earlier findings of Holzwarth *et al.*<sup>10</sup> Nonetheless, the reaction energy for Eqn. (1) is only -25 meV / atom, indicating that it can be easily stabilized by entropic effects, or created as a metastable phase.

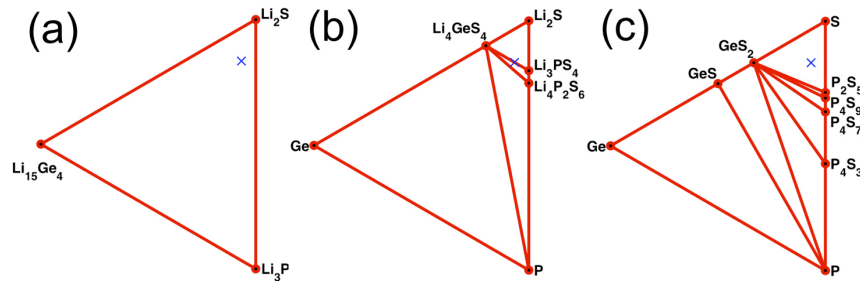


FIGURE 1. Phase evolution of Li-Ge-P-S system as a function of Li chemical potential  $\mu_{\text{Li}}$  at (a) 0 eV, (b) -1.8 eV and (c) -2.5 eV.  $\mu_{\text{Li}} = 0$  eV corresponds to metallic Li. Labelled dots denote stable phases at each  $\mu_{\text{Li}}$ . For all other compositions, the equilibrium state is formed by a combination of the stable phases in the triangle surrounding that composition. The LGPS composition is marked with a blue cross. For example, the equilibrium state of the LGPS composition is given by a combination of  $\text{GeS}_2$ , S and  $\text{P}_2\text{S}_5$  at  $\mu_{\text{Li}} = -2.5$  eV.

Using the methodology outlined in Ong *et al.*,<sup>11</sup> we plotted the lithium grand potential phase diagrams of the Li-Ge-P-S system at various lithium chemical potentials ( $\mu_{\text{Li}}$ ) of interest in Figure 1. Lithium grand potential phase diagrams represent the phase equilibria of a Li-Ge-P-S system that is open to lithium, which is relevant when the LGPS solid electrolyte is in contact with a reservoir of lithium, as is the case in a lithium battery. The voltage in a battery is the negative of the Li chemical potential. The Li chemical potentials in Figure 1 were chosen to elucidate the key changes in the equilibrium decomposition of LGPS as we go from the bulk metallic Li chemical potential (Figure 1(a)) to an environment where no Li-containing phases are present in the phase diagram (Figure 1(c)).

From Figure 1(a), we may observe that at the metallic lithium chemical potential, we predict that the LGPS solid electrolyte will consume lithium to decompose to a combination of  $\text{Li}_2\text{S}$ ,  $\text{Li}_3\text{P}$  and  $\text{Li}_{15}\text{Ge}_4$ . At  $-1.8 \text{ eV} < \mu_{\text{Li}} < -2.4 \text{ eV}$  (Figure 1(b)), LGPS decomposes via the equilibrium decomposition in Eqn. (1). Finally, at even lower  $\mu_{\text{Li}} > -2.4 \text{ eV}$  (Figure 1(c)), LGPS decomposes into  $\text{P}_2\text{S}_5$ , S and  $\text{GeS}_2$  with lithium extraction. Though Kamaya *et al.*<sup>3</sup> reported that LGPS is stable for an electrochemical window in excess of 5 V vs  $\text{Li}/\text{Li}^+$  with no observed electrolyte decomposition currents in that range, our calculations indicate that this material is unlikely to be stable against lithium. We propose that an alternative explanation for the wide electrochemical window of LGPS is that the decomposition of this material in contact with the electrodes result in the formation of either  $\text{Li}_2\text{S}$  (anode) or  $\text{P}_2\text{S}_5$  (cathode), possibly in an amorphous form, which are components of the well-known glassy Li-ion conductors.<sup>12</sup> The formation of such a Li-conducting passivation layer would prevent further decomposition of the electrolyte with minimal impact on electrochemical performance. A similar solid electrolyte interphase (SEI) phenomenon has indeed been reported by Kobayashi *et al.*<sup>13</sup> for the similar  $\text{Li}_{3.25}\text{Ge}_{0.25}\text{P}_{0.75}\text{S}_4$  thio-LISICON.

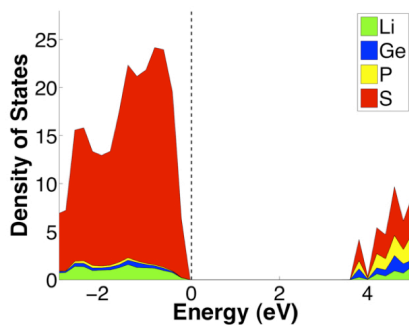


FIGURE 2. DOS of LGPS calculated with the HSE06 functional.

We also calculated the electrochemical window of LGPS on inert electrodes using the approach outlined by Ong *et al.*<sup>14</sup> Briefly, the approach involves the calculation of the density of states (DOS) of LGPS to determine the lowest unoccupied molecular orbital (LUMO) and highest occupied molecular orbital (HOMO) energies. Given the known limitations of GGA functionals in calculating band gaps, the DOS of LGPS was calculated using the Heyd-Scuseria-Ernzerhof (HSE06) functional<sup>15</sup> and is given in Figure 2. We find that the HSE06 band gap is calculated to be around 3.6 eV, far smaller than the electrochemical window of  $> 5 \text{ V}$  reported by Kamaya *et al.* Because the electrochemical window estimated using this

approach is an upper limit assuming inert electrodes, this result lends further credence to our hypothesis that the excellent electrochemical stability of LGPS is not due to the intrinsic stability of the material itself, but rather the result of passivation phenomenon.<sup>13</sup> We believe that the loss of Coulombic efficiency in the first cycles of the solid state battery constructed with LGPS<sup>3</sup> is evidence of lithium consumption, which creates the interfacial decomposition products.

To study the Li diffusion in LGPS, we performed *ab initio* molecular dynamics (MD) simulations under the Born-Oppenheimer approximation. The MD simulations were performed at elevated temperatures (600K to 1500K) to speed up diffusion and shorten the simulation timescale. The time step was chosen to be 2 fs and the diffusion simulations were performed for 40 ps. No breaking of P-S or Ge-S bonds was observed during the simulations. More details about the simulations can be found in the Supporting Information.

The trajectories of Li diffusion during the *ab initio* MD simulations are shown in Figure 3. From our simulations, we observe very facile Li diffusion in the 1D diffusion channels along the  $c$  direction (Figure 3 (a)). This diffusion pathway is consistent with the hypothesis of Kamaya *et al.*<sup>3</sup> However, we also find significant Li hopping in the  $ab$  plane. Figure 3(b) shows one of these new diffusion pathways, which connect one  $\text{LiS}_4$  tetrahedra to another  $\text{LiS}_4$  tetrahedra in the diagonal directions in the  $ab$  plane. The diffusion in the  $ab$  plane is not surprising, because there is empty space for diffusion between the  $(\text{Ge}_{0.5}\text{P}_{0.5})\text{S}_4$  tetrahedra and  $\text{PS}_4$  tetrahedra (Figure 3 (a)). Yet another diffusion pathway connects Li atoms in  $\text{LiS}_6$  octahedra site to the  $c$ -axis diffusion channels (Figure 3(c)). This pathway in the  $ab$  plane connects the  $\text{LiS}_4$  tetrahedra site to the  $\text{LiS}_6$  octahedra site, which was originally regarded by Kamaya *et al.* as inactive for diffusion.

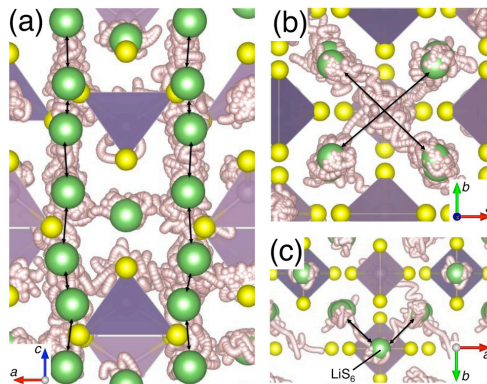


FIGURE 3. Trajectories (white) of Li atoms (Green) in *ab initio* MD simulations at 900K. The 1D diffusion pathway along the  $c$  direction (a); and diffusion in the  $ab$  plane (b) & (c).  $\text{PS}_4$  ( $\text{GeS}_4$ ) tetrahedra in light (dark) purple. S atoms in yellow. The initial positions of non-diffusing atoms and all Li sites are shown for ease of visualization.

We calculated the diffusion coefficients for all pathways found by the MD simulations. The diffusion coefficient is calculated as the averaged mean square displacement of Li atoms over time. Convergence of diffusion coefficients is achieved with approximately 40 ps of MD simulations because of the relatively fast Li diffusion in this material. Figure 4 shows the Arrhenius plot for the various diffusion coefficients at temperatures from 600K to 1500K. From Figure 4(a), we calculate an overall activation barrier of 0.21 eV for Li diffu-

sion in LGPS. This calculated barrier is in remarkable agreement with the experimentally determined barrier of 0.24 eV,<sup>3</sup> despite the fact that the *ab initio* MD calculations were carried out at much higher temperatures than the experiments. The calculated diffusion extrapolates to a Li<sup>+</sup> conductivity of 9 mS/cm (with a range of 2 to 40 mS/cm) at 300K, which again is in remarkable agreement with the experimental conductivity of 12 mS/cm.

From Figure 4(b), we may observe that Li diffusion along the *c* direction is faster than the diffusion in the *ab* plane. We calculate activation barriers of 0.17 eV for the diffusivity in the *c* direction  $D_c$  and 0.28 eV for the diffusivity in the *ab* plane  $D_{ab}$ . Extrapolating from the Arrhenius plot, we find that  $D_c$  is predicted to be two orders of magnitude higher than  $D_{ab}$  at 300K. The extrapolated conductivity at 300K is around 40 mS/cm in the *c* direction and 0.9 mS/cm in the *ab* plane.

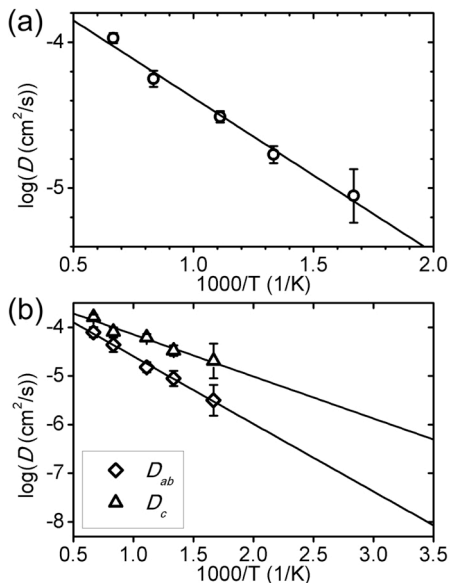


FIGURE 4. Arrhenius plot of (a) overall diffusion coefficient and the diffusion coefficient in the *c* direction  $D_c$  and in the *ab* plane  $D_{ab}$ . (b). The error bar corresponds to statistical uncertainty in the fitting the mean square displacement to time curve.

Our simulations show that LGPS is in fact a 3D ion conductor rather than a 1D ion conductor. The 3D diffusion network consists of 1D diffusion channels along the *c* direction and inter-channel diffusion in the *ab* plane. This difference between 3D and 1D is significant as truly 1D conductors can not retain their good conductivity in the macroscopic limit due the inevitable presence of channel blocking defects<sup>16</sup> and some cross-over between 1D channels is required to bypass such defects. The fact that the activation energy for the overall Li diffusivity is between the activation energy for *c*-axis and *ab*-plane motion evidences that such crossovers are important for the overall transport. While diffusivity is predicted to be two orders of magnitude more facile in the *c* direction as compared to the *ab* directions at 300K, there is nonetheless significant diffusion in the *ab* plane as well. The predicted conductivity in the *ab* plane at 300K is as high as ~1 mS/cm, which is still comparable with state-of-the-art solid electrolytes.

In summary, we investigated the LGPS lithium super ionic conductor material using a variety of first principles techniques. We find that LGPS is a metastable phase in the calculated phase diagram. We also find that LGPS is not stable

against reduction by lithium at low voltage or extraction of Li with decomposition at high voltage. Together with the calculated band gap of 3.6 eV, these predictions suggest that the observed electrochemical window greater than 5V of this material is likely the result of passivation phenomenon where either Li<sub>2</sub>S or P<sub>2</sub>S<sub>5</sub> is formed as a decomposition product.

Our *ab initio* MD simulations confirm fast Li diffusion in the 1D diffusion channel along the *c* direction, but also predict two additional diffusion pathways in the *ab* plane. Though diffusion in the *ab* plane is not as facile as in the *c* direction, it nonetheless contributes to the overall performance of the material. Our calculated overall activation barrier and conductivity are in remarkable agreement with the experimental values.

## ASSOCIATED CONTENT

**Supporting Information.** Computational details. This material is available free of charge via the Internet at <http://pubs.acs.org>.

## AUTHOR INFORMATION

### Corresponding Author

\* E-mail: [gceder@mit.edu](mailto:gceder@mit.edu)

## ACKNOWLEDGMENT

We would like to thank the Samsung Advanced Institute of Technology for their funding of this research. We also thank Lincoln Miara and Hyo Sug Lee for helpful discussions.

## ABBREVIATIONS

LGPS, Li<sub>10</sub>GeP<sub>2</sub>S<sub>12</sub>; MD, molecular dynamics; SEI, solid electrolyte interphase; GGA, generalized-gradient approximation; HSE06, Heyd-Scuseria-Ernzerhof; DOS, density of states.

## REFERENCES

- Armand, M.; Tarascon, J. M., *Nature* **2008**, 451, (7179), 652-657.
- Tarascon, J. M.; Armand, M., *Nature* **2001**, 414, (6861), 359-367.
- Kamaya, N.; Homma, K.; Yamakawa, Y.; Hirayama, M.; Kanno, R.; Yonemura, M.; Kamiyama, T.; Kato, Y.; Hama, S.; Kawamoto, K.; Mitsui, A., *Nat Mater* **2011**, 10, (9), 682-686.
- Kresse, G.; Furthmuller, J., *Phys. Rev. B* **1996**, 54, (16), 11169-11186.
- Blöchl, P. E., *Phys. Rev. B* **1994**, 50, (24), 17953-17979.
- Perdew, J. P.; Ernzerhof, M.; Burke, K., *J. Chem. Phys.* **1996**, 105, (22), 9982-9985.
- Bergerhoff, G.; Hundt, R.; Sievers, R.; Brown, I. D., *J. Chem. Inf. Comput. Sci.* **1983**, 23, (2), 66-69.
- Ewald, P. P., *Ann. Phys.-Berlin* **1921**, 64, (3), 253-287.
- Jain, A.; Hautier, G.; Moore, C. J.; Ong, S. P.; Fischer, C. C.; Mueller, T.; Persson, K. A.; Ceder, G., *Computational Materials Science* **2011**, 50, (8), 2295-2310.
- Holzwarth, N. A. W.; Lepley, N. D.; Du, Y. A., *Journal of Power Sources* **2011**, 196, (16), 6870-6876.
- Ong, S. P.; Wang, L.; Kang, B.; Ceder, G., *Chem. Mat.* **2008**, 20, (5), 1798-1807.
- Murayama, M.; Sonoyama, N.; Yamada, A.; Kanno, R., *Solid State Ionics* **2004**, 170, (3-4), 173-180.
- Kobayashi, T.; Yamada, A.; Kanno, R., *Electrochimica Acta* **2008**, 53, (15), 5045-5050.
- Ong, S. P.; Andreussi, O.; Wu, Y.; Marzari, N.; Ceder, G., *Chem. Mat.* **2011**, 23, (11), 2979-2986.
- Heyd, J.; Scuseria, G. E.; Ernzerhof, M., *J. Chem. Phys.* **2003**, 118, (18), 8207-8215.
- Malik, R.; Burch, D.; Bazant, M.; Ceder, G., *Nano Letters* **2010**, 10, (10), 4123-4127.